

# Towards Clustering-friendly Representations: Subspace Clustering via Graph Filtering

Zhengrui Ma  
Zhao Kang\*

School of Computer Science and  
Engineering, University of Electronic  
Science and Technology of China  
zkang@uestc.edu.cn

Guangchun Luo

School of Information and Software  
Engineering, University of Electronic  
Science and Technology of China  
gcluo@uestc.edu.cn

Ling Tian, Wenyu Chen

School of Computer Science and  
Engineering, University of Electronic  
Science and Technology of China  
{lingtian,cwy}@uestc.edu.cn

## ABSTRACT

Finding a suitable data representation for a specific task has been shown to be crucial in many applications. The success of subspace clustering depends on the assumption that the data can be separated into different subspaces. However, this simple assumption does not always hold since the raw data might not be separable into subspaces. To recover the “clustering-friendly” representation and facilitate the subsequent clustering, we propose a graph filtering approach by which a smooth representation is achieved. Specifically, it injects graph similarity into data features by applying a low-pass filter to extract useful data representations for clustering. Extensive experiments on image and document clustering datasets demonstrate that our method improves upon state-of-the-art subspace clustering techniques. Especially, its comparable performance with deep learning methods emphasizes the effectiveness of the simple graph filtering scheme for many real-world applications. An ablation study shows that graph filtering can remove noise, preserve structure in the image, and increase the separability of classes.

## CCS CONCEPTS

• **Computing methodologies** → **Spectral methods; Cluster analysis**; • **Mathematics of computing** → **Spectra of graphs; Graph algorithms**.

## KEYWORDS

Subspace clustering, graph filtering, representation learning, smooth representation.

## ACM Reference Format:

Zhengrui Ma, Zhao Kang, Guangchun Luo, and Ling Tian, Wenyu Chen. 2020. Towards Clustering-friendly Representations: Subspace Clustering via Graph Filtering. In *Proceedings of the 28th ACM International Conference on Multimedia (MM '20)*, October 12–16, 2020, Seattle, WA, USA. ACM, New York, NY, USA, 9 pages. <https://doi.org/10.1145/3394171.3413597>

\*Corresponding author

Permission to make digital or hard copies of all or part of this work for personal or classroom use is granted without fee provided that copies are not made or distributed for profit or commercial advantage and that copies bear this notice and the full citation on the first page. Copyrights for components of this work owned by others than the author(s) must be honored. Abstracting with credit is permitted. To copy otherwise, or republish, to post on servers or to redistribute to lists, requires prior specific permission and/or a fee. Request permissions from [permissions@acm.org](mailto:permissions@acm.org).

MM '20, October 12–16, 2020, Seattle, WA, USA

© 2020 Copyright held by the owner/author(s). Publication rights licensed to ACM. ACM ISBN 978-1-4503-7988-5/20/10...\$15.00  
<https://doi.org/10.1145/3394171.3413597>

## 1 INTRODUCTION

Clustering is a long-standing problem in machine learning, data mining, and pattern recognition, with an endless of applications. It is also a notoriously hard task due to its unsupervised learning nature [12, 28, 45]. Its performance can be easily affected by many factors, such as data representation, feature dimension, and noise [4, 8, 11, 13]. Among various clustering techniques, K-means and spectral clustering are especially popular.

K-means is suitable for data that are evenly spread around some centroids [21, 22, 27]. In many real-life applications, the data might not be separable. A number of techniques, including kernel trick, principal component analysis, canonical correlation analysis, have been developed to map high-dimensional data to a certain representation that is suitable for performing K-means. Spectral clustering is basically a generalization of kernel K-means [24, 36]. They provide meaningful outputs only when the data are mapped to a “clustering-friendly” representation, in which the data samples nicely fall into clusters.

To tackle the curse of dimensionality, subspace clustering (SC) assumes that data lie in a union of subspaces [20, 31]. SC has well-documented impact in a wide range of applications [43]. It has been pointed out that applying subspace clustering on the projected data is beneficial since the original data might not fall on separate subspaces [19, 26].

In this paper, instead of applying subspace clustering on the original space, we learn the subspace clustering in a “clustering-friendly” representation, which is easy to cluster. Even if the data cannot be separated in the original domain, its smooth representation can be grouped into disjoint subspaces. In particular, we inject graph similarity into data features by applying a low-pass filter to extract meaningful data representations for clustering. Since the graph is unavailable beforehand, an iterative approach is used. The proposed framework can incorporate various subspace clustering models.

Our contributions are summarized as follows.

- We propose a graph filtering framework for subspace clustering, which generates a “clustering-friendly” representation. This provides a new representation learning strategy.
- Taking two representative subspace clustering techniques as examples, we demonstrate the considerable enhancement brought by graph filtering on a number of datasets.
- Graph filtering approach produces comparable results with respect to state-of-the-art deep neural networks based clustering techniques.

- An ablation study shows that graph filtering can remove noise, preserve structure in the image, and increase the separability of classes.

## 2 GRAPH FILTERING

Suppose an undirected graph  $G = (\mathcal{V}, W, X)$  with  $n = |\mathcal{V}|$  vertices is given, with an edge weights matrix  $W \in \mathcal{R}^{n \times n}$ , where  $w_{ij} = w_{ji} \geq 0$ , and a feature matrix  $X = [\mathbf{x}_1, \dots, \mathbf{x}_n]^\top \in \mathcal{R}^{n \times m}$  corresponding to  $n$  vertices. The degree of vertex  $v_i$  is defined as  $D_{ii} = \sum_{j=1}^n w_{ij}$  and  $D = \text{diag}(d_1, \dots, d_n)$ . The symmetrically normalized graph Laplacian  $L_s = I - D^{-\frac{1}{2}} W D^{-\frac{1}{2}}$  can be eigen-decomposed as  $L_s = U \Lambda U^{-1}$ , where the associated eigenvalues  $\Lambda = \text{diag}(\lambda_1, \dots, \lambda_n)$  are sorted in increasing order and  $U = [\mathbf{u}_1, \dots, \mathbf{u}_n]$  are the corresponding orthogonal eigenvectors. The set of eigenvectors of  $L_s$  can be considered as Fourier basis of the graph and the eigenvalues  $\lambda_i$  can be considered as the associated frequencies [30].

Let  $f : \mathcal{V} \rightarrow \mathbb{R}$  be a real-valued function on the nodes of a graph, a *graph signal*  $\mathbf{f} = [f(v_1), f(v_2), \dots, f(v_n)]^\top$  can be represented as a linear combination of the eigenvectors, i.e.,

$$\mathbf{f} = \sum_{i=1}^n c_i \mathbf{u}_i = U \mathbf{c}, \quad (1)$$

where  $\mathbf{c} = [c_1, c_2, \dots, c_n]^\top$  is the coefficient vector. The absolute value of  $c_i$  shows the strength of the basis signal  $\mathbf{u}_i$  presented in graph signal  $\mathbf{f}$ . The smoothness of  $\mathbf{f}$  can be measured by

$$\begin{aligned} E_f &= \frac{1}{2} \sum_{i,j=1}^n w_{ij} \left\| \frac{f_i}{\sqrt{d_i}} - \frac{f_j}{\sqrt{d_j}} \right\|_2^2 = \mathbf{f}^\top L_s \mathbf{f} \\ &= (U \mathbf{c})^\top L_s U \mathbf{c} = \sum_{i=1}^n c_i^2 \lambda_i. \end{aligned} \quad (2)$$

This indicates that the basis signals corresponding to smaller  $\lambda_i$  are smoother. Hence, a smooth signal  $\mathbf{f}$  should consist of more low-frequency basis signals than high-frequency ones [1].

The graph signals associated with the real-world data should be sufficiently smooth, i.e., the signal values should change gradually across connected neighbor nodes. This can be achieved through a low-pass graph filter  $G$ . Assume  $h(\lambda_i)$  is a low-pass frequency response function, the filtered signal  $\tilde{\mathbf{f}}$  can be written as

$$\tilde{\mathbf{f}} = G \mathbf{f} = \sum_{i=1}^n h(\lambda_i) c_i \mathbf{u}_i = U H(\Lambda) \mathbf{c} = U H(\Lambda) U^{-1} \mathbf{f}, \quad (3)$$

where  $H(\Lambda) = \text{diag}(h(\lambda_1), h(\lambda_2), \dots, h(\lambda_n))$ . To preserve the low-frequency signals and remove the high-frequency ones,  $h(\lambda_i)$  should be large for small  $\lambda_i$  and vice versa. Since the eigenvalues of symmetrically normalized graph Laplacian  $L_s$  fall to range  $[0, 2]$ , one choice of the low-pass response function is  $h(\lambda_i) = (1 - \frac{\lambda_i}{2})^k$ , where positive integer  $k$  is applied to capture the  $k$ -hop neighborhood relations [1, 44]. Then the filtered signal can be formulated as

$$\tilde{\mathbf{f}} = U \left( I - \frac{\Lambda}{2} \right)^k U^{-1} \mathbf{f} = \left( I - \frac{L_s}{2} \right)^k \mathbf{f}. \quad (4)$$

Each column of  $X$  can be taken as a graph signal. Then, a smoothed representation  $\bar{X}$  is achieved by

$$\bar{X} = \left( I - \frac{L_s}{2} \right)^k X. \quad (5)$$

In essence,  $\bar{x}_i$  is obtained by aggregating the features of its  $k$ -hop neighbors iteratively. Thus, a  $k$ -order graph filtering takes into account long-distance data relations, which would be useful for capturing global structure to improve downstream task performance.

## 3 THE PROPOSED METHODOLOGY

Samples drawn from the same cluster tend to be densely connected, thus it is natural to assume that they are likely to have similar feature representations [33]. To this end, we can obtain ‘‘clustering-friendly’’ representations by using graph filtering.

Subspace clustering constructs an affinity graph matrix  $W$  from feature matrix  $X$  for the subsequent spectral clustering task. In this work, we aim to learn  $W$  in a smooth representation  $\bar{X}$ . However, to compute  $\bar{X}$ , we need to know the affinity graph  $W$  in advance. To address this dilemma, we propose an iterative approach.

Our proposed graph filtering perspective can be generally integrated with various kinds of subspace clustering models. Due to its simplicity and effectiveness, Least Square Regression (LSR) is a very popular subspace clustering model as shown in Eq.(17) in [23]. Hence, we choose it to demonstrate our proposed method. Suppose we have smooth representation  $\bar{X}$ , LSR learns a coefficient matrix  $Z$  by

$$\min_Z \|\bar{X}^\top - \bar{X}^\top Z\|_F^2 + \alpha \|Z\|_F^2. \quad (6)$$

Its closed-form solution can be achieved by setting its first-order derivative to zero, which yields

$$Z = (\bar{X} \bar{X}^\top + \alpha I)^{-1} \bar{X} \bar{X}^\top. \quad (7)$$

Since

$$\begin{aligned} Z^\top &= \bar{X} \bar{X}^\top (\bar{X} \bar{X}^\top + \alpha I)^{-1} \\ &= (\bar{X} \bar{X}^\top + \alpha I - \alpha I) (\bar{X} \bar{X}^\top + \alpha I)^{-1} \\ &= I - \alpha (\bar{X} \bar{X}^\top + \alpha I)^{-1} \\ &= (\bar{X} \bar{X}^\top + \alpha I)^{-1} (\bar{X} \bar{X}^\top + \alpha I - \alpha I) = Z, \end{aligned} \quad (8)$$

we can directly set  $W = |Z|$ , which in turn can be used to update  $\bar{X}$ . To start the iterative algorithm, smooth representation  $\bar{X}$  can be initialized to raw feature matrix  $X$ , so that an initial graph  $W$  can be achieved by Eq. (7). We can stop the iterations when the difference between affinity matrices obtained in the  $t$ -th and  $(t+1)$ -th iteration is smaller than a threshold  $\epsilon$ , i.e.,  $\|W_t - W_{t-1}\|_F^2 < \epsilon$ . Afterwards, the spectral clustering is utilized upon  $W$ . The complete procedure for our algorithm is outlined in Algorithm 1.

In Algorithm 1, the cost for updating  $Z$  is  $\mathcal{O}(\max(m, n)n^2)$ . Updating  $W$  takes  $\mathcal{O}(n^2)$ . To compute  $L$ , we need  $\mathcal{O}(n^2)$  time. The cost for updating  $\bar{X}$  is  $\mathcal{O}(n^3)$ . Hence, the overall complexity is  $\mathcal{O}(t(\max(m, n)n^2))$ , where  $t$  is the number of iterations. In fact, our method can be easily modified to deal with large-scale data. For the graph filtering part, since the graph is often sparse (Let  $N, d$  denote the number of nonzero entries in graph Laplacian and feature dimensions respectively), we can left multiply  $X$  by  $(I - \frac{L_s}{2})$  for  $k$  times, resulting in  $\mathcal{O}(Ndk)$ . For subspace clustering part, we can

---

**Algorithm 1** FLSR

---

**Input:** raw feature matrix  $X$ **Parameter:** filter order  $k$ , trade-off parameter  $\alpha$ , cluster number  $g$ **Output:**  $g$  partitions

- 1: Initialize  $t = 0$  and  $\bar{X}_1 = X$
  - 2: **repeat**
  - 3:   Set  $t = t + 1$ .
  - 4:    $Z_t = (\bar{X}_t \bar{X}_t^\top + \alpha I)^{-1} \bar{X}_t \bar{X}_t^\top$
  - 5:    $W_t = \text{abs}(Z_t)$
  - 6:    $L_t = I - D_t^{-\frac{1}{2}} W_t D_t^{-\frac{1}{2}}$
  - 7:    $\bar{X}_{t+1} = (I - \frac{1}{2} L_t)^k X_t$
  - 8: **until**  $\|W_t - W_{t-1}\|_F^2 < \epsilon$
  - 9: Obtain the cluster partitions by performing spectral clustering on  $W$
- 

perform it in  $O(n)$  time by the idea of anchor point [15]. Scalability is left for future work.

Based on LSR, Thresholding Ridge Regression (TRR) [29] was proposed later. According to the property of intra-subspace projection dominance, coefficients of two samples from one cluster in learned affinity matrix by LSR are always larger than coefficients of samples from different clusters. Therefore, an extra step can be added before spectral clustering. We can only preserve first  $p$  largest values in each row of affinity matrix  $W$ , where the value of  $p$  can be the dimensionality of subspace. For convenience, we name graph filtering based LSR and TRR as FLSR and FTTR, respectively.

## 4 EXPERIMENT

In this section, we conduct experiments to demonstrate the effectiveness of graph filtering in subspace clustering<sup>1</sup>.

### 4.1 Dataset

We perform clustering experiments on three face datasets (ORL, AR and Umist), two object datasets (COIL20 and COIL40), one handwritten digit dataset (MNIST) and one large scale news dataset (RCV1). Specifically, ORL is composed of 400 images with different poses and expressions from 40 individuals. AR has 840 samples from 120 subjects. Umist contains 480 images with varied poses from 20 individuals. COIL20 and COIL40 have 20 and 40 classes respectively, with each class having 72 toy images. MNIST comprises handwritten digit images of 0 to 9. We use first 100 images of each digit. There are 9625 news texts in RCV1. The statistics information is summarized in Table 1.

### 4.2 Experimental Setup

Several representative models in subspace clustering are compared in our experiment, including Sparse Subspace Clustering (SSC) [3], Low Rank Representation (LRR) [18], Latent Low Rank Representation (LatLRR) [19], Low Rank Subspace Clustering (LRSC) [32], Least Square Regression [23], Thresholding Ridge Regression (TRR) [29], Sparse Subspace Clustering by Orthogonal Matching Pursuit (SSCOMP) [42], Discriminative Unsupervised Dimensionality

**Table 1: Statistics of datasets.**

Dataset	Samples	Classes	Dimensions
ORL	400	40	1024
AR	840	120	768
Umist	480	20	1024
COIL20	1440	20	1024
COIL40	2880	40	1024
MNIST	1000	10	784
RCV1	9625	4	29992

Reduction (DUDR) [34], Scaled Simplex Representation based Subspace Clustering (SSRSC) [39]. In particular, SSRSC was published in 2019 and has shown better performance than RSIM [9], SMR [7], S3C [16], EnSC [41], ESC [40], etc. Hence, we do not compare with those methods. Additionally, similar to our approach, both LatLRR and DUDR perform subspace clustering in a new representation.

For fair comparison, we apply the same postprocessing step in all models. Specifically, affinity graph is constructed as the following

$$W = \frac{|Z^\top| + |Z|}{2}. \quad (9)$$

Then spectral clustering algorithm is implemented. Parameters in each model are well-tuned to achieve its best clustering results. For our FLSR and FTTR, we fix the threshold  $\epsilon$  to  $10^{-5}$  and search for proper trade-off parameter  $\alpha$  and filter order  $k$ . For FTTR, we additionally search for a proper threshold parameter  $p$ , the value of which is recommended to be the dimensionality of subspace [29].

Three popular metrics are applied to quantitatively evaluate the clustering performance. They are accuracy (ACC), normalized mutual information (NMI), and purity (PUR).

Accuracy is defined as

$$ACC = \frac{\sum_i \delta(\text{map}(l_i) = y_i)}{n} \quad (10)$$

where  $y_i$  and  $l_i$  denote the ground truth label and algorithm's output of sample  $i$ .  $\delta(\cdot)$  is the indicator function.  $l_i$  is mapped to its best group label with Kuhn-Munkres algorithm.

Normalized mutual information is defined as

$$NMI(Y, L) = \frac{I(Y, L)}{\sqrt{H(Y)H(L)}} \quad (11)$$

where  $Y$  and  $L$  denote the ground truth labels and algorithm's output.  $I(\cdot)$  is the mutual information which measures the information gain after knowing the partitions generated by algorithm. The entropy of  $Y$  and  $L$  are used for normalization purpose.

Purity is defined as

$$PUR(Y, L) = \frac{\sum_i \max_j |L_i \cap Y_j|}{n} \quad (12)$$

where  $L = \{L_1, L_2, \dots, L_c\}$  denotes the partition of clusters generated by algorithm and  $Y = \{Y_1, Y_2, \dots, Y_c\}$  denotes the ground truth of clusters. Each cluster generated by algorithm is assigned to a real cluster which has the most same samples.

<sup>1</sup>The source code is available at <https://github.com/sckangz/STRR>

**Table 2: Clustering results of various methods on ORL, AR, Umist, COIL20, COIL40, MNIST, and RCV1. For RCV1, some methods which need a long running time are ignored.**

Dataset	Metric	SSC	LRR	SSCOMP	LRSC	SSRSC	LatLRR	DUDR	LSR	TRR	FLSR	FTRR
ORL	ACC	56.00	72.25	39.00	74.50	77.75	72.75	61.75	71.50	83.25	77.75	<b>86.00</b>
	NMI	70.06	83.42	58.95	83.47	86.53	85.81	73.83	82.57	91.11	86.61	<b>91.51</b>
	PUR	62.00	76.25	47.00	76.50	78.50	76.75	67.50	76.25	<b>87.50</b>	79.00	87.25
AR	ACC	42.86	74.64	29.29	77.02	72.26	76.67	40.65	71.67	83.10	72.38	<b>89.76</b>
	NMI	63.57	87.22	52.34	86.03	88.19	89.19	61.05	87.70	93.22	88.13	<b>94.64</b>
	PUR	49.88	77.50	36.19	79.40	75.36	79.29	43.69	74.88	84.52	75.95	<b>90.48</b>
COIL20	ACC	76.60	58.33	39.31	60.63	74.51	65.69	81.46	68.68	83.89	71.04	<b>90.35</b>
	NMI	88.09	71.19	53.38	72.28	82.92	76.76	87.05	74.10	90.94	78.47	<b>93.05</b>
	PUR	83.47	61.67	78.26	62.22	77.50	69.65	83.06	70.90	<b>92.85</b>	75.07	91.04
COIL40	ACC	63.13	60.42	18.92	58.23	57.01	60.52	69.13	56.88	78.37	59.20	<b>78.58</b>
	NMI	82.82	76.29	29.49	74.48	73.11	75.96	80.49	75.87	87.98	75.54	<b>88.01</b>
	PUR	72.05	62.81	23.16	64.24	60.94	64.24	75.10	62.74	<b>85.31</b>	62.27	81.56
Umist	ACC	64.79	61.67	28.75	60.63	66.88	61.25	69.38	60.21	70.83	60.00	<b>76.67</b>
	NMI	75.38	72.95	41.11	72.08	75.14	70.27	77.42	71.58	77.86	70.82	<b>85.09</b>
	PUR	66.25	64.17	38.54	63.33	68.54	62.50	74.17	62.71	73.33	61.88	<b>79.17</b>
MNIST	ACC	55.60	58.60	34.00	59.10	55.80	59.80	56.30	55.50	60.50	62.10	<b>70.70</b>
	NMI	50.14	54.69	32.72	52.75	52.74	55.50	47.94	54.96	56.34	52.31	<b>66.72</b>
	PUR	55.60	62.50	35.60	62.50	57.50	63.40	56.30	58.90	61.00	62.10	<b>70.70</b>
RCV1	ACC	-	-	30.23	-	-	-	-	64.06	71.01	77.54	<b>81.85</b>
	NMI	-	-	2.86	-	-	-	-	42.05	48.66	54.89	<b>59.66</b>
	PUR	-	-	32.68	-	-	-	-	64.06	80.16	<b>82.65</b>	81.85

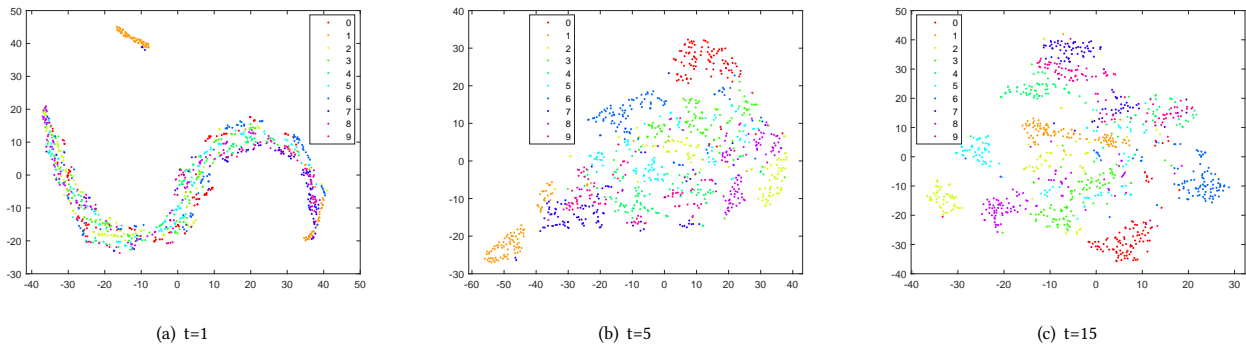


**Figure 1: t-SNE demonstration of filtered features of MNIST during the iteration process.**

### 4.3 Results

The results of experiments are summarized in Table 2, where the best results are highlighted in bold. We can observe that our purposed graph filtering framework boosts the performance of state-of-the-art subspace clustering techniques across most evaluation metrics. In particular,

- FLSR and FTRR evidently improve the clustering results compared with the models they built upon. For example, FLSR and FTRR improve the accuracy of LSR and TRR by 4.47% and 6.14% respectively. This is attributed to the adoption

of "clustering-friendly" representations realized by graph filtering. In particular, spatially close data points may help each other to prevent over-fitting in reconstructing the samples, i.e., the first term in Eq. (6). We use t-SNE to visualize the evolution of representation  $\tilde{X}$  as the iteration goes on in Fig.1. As we can see, the filtered representation displays clearer cluster structure as the process goes on. The grouping effect of the filtered representation makes it much easier to separate the data points into disjoint subspaces.

**Table 3: Clustering results of FLSR and FTRR compared with deep methods.**

Dataset	Metric	AE-SSC	DSC-L1	DEC	DKM	DCCM	FLSR	FTRR
ORL	ACC	75.63	85.50	51.75	46.82	60.00	77.75	<b>86.00</b>
	NMI	85.55	90.23	74.49	73.32	79.30	86.61	<b>91.51</b>
	PUR	79.50	85.85	54.00	47.52	56.30	79.00	<b>87.25</b>
COIL20	ACC	87.11	<b>93.14</b>	72.15	66.51	81.40	71.04	90.35
	NMI	89.90	<b>93.53</b>	80.07	79.71	87.10	78.47	93.05
	PUR	89.01	<b>93.06</b>	69.31	69.64	80.10	75.07	91.04
COIL40	ACC	73.91	<b>80.03</b>	48.72	58.12	78.00	59.20	78.58
	NMI	83.18	88.52	74.17	78.40	<b>89.10</b>	75.54	88.01
	PUR	78.40	<b>86.46</b>	41.63	63.67	77.10	62.27	81.56
Umist	ACC	70.42	72.42	55.21	51.06	54.00	60.00	<b>76.67</b>
	NMI	75.15	75.56	71.25	82.49	74.30	70.82	<b>85.09</b>
	PUR	67.85	72.04	59.17	56.85	58.30	61.88	<b>79.17</b>
MNIST	ACC	48.40	<b>72.80</b>	61.20	53.32	42.50	62.10	70.70
	NMI	53.37	<b>72.17</b>	57.43	50.02	37.70	52.31	66.72
	PUR	52.90	<b>78.90</b>	63.20	56.47	45.00	62.10	70.70

- Compared to most recent method SRLSR, FTRR consistently outperforms it by a large margin. On average, accuracy, NMI, and purity are improved by 14.64%, 10.07%, and 13.64%, respectively.
- FLSR clearly outperforms LatLRR on ORL, COIL20, and is comparable on COIL40 and Umist. Note that LatLRR performs learning in latent space, which can extract salient features from hidden data, and thus can work much better than the benchmark methods that use the original data as features. Moreover, it demonstrates that LatLRR is more robust to noise with respect to dimension reduction based methods. Though LatLRR often performs better than LSR, its inferior to FLSR verifies that graph filtering is powerful.
- FTRR consistently outperforms LatLRR and DUDR by a very large margin. DUDR simultaneously performs dimension reduction and affinity graph construction. This shows that graph filtering could be more effective than dimension reduction approach in representation learning.

Take ORL as an example, we show the learned affinity graph matrix  $W$  in Fig. 2. Ideally, it should have a block-diagonal structure. As observed, both TRR and FTRR produce high-quality graphs. However, FTRR generates less noise than TRR. This explains why FTRR generates higher values in terms of accuracy, NMI, and purity.

In Fig. 3, we also plot the change of accuracy, NMI, and purity values of FLSR as the iteration goes on. We can see that the performance increases quickly in the first 5 iterations and it reaches convergence after 7 iterations. Hence, we can see that our algorithm converges fast. Furthermore, the small fluctuations on the curve could be explained by the iterative nature of our algorithm.

#### 4.4 Parameter Analysis

There is a trade-off parameter  $\alpha$  in model (6). In addition, there is an implicit parameter  $k$ , i.e., the order of the filter. When  $k$  increases,



(a) TRR



(b) FTRR

**Figure 2: Affinity graph matrix obtained on ORL dataset.**

nearby node features become similar. However, too large  $k$  will result in over-smoothing, i.e., the features of nodes in different clusters are mixed and become indistinguishable. Therefore, too large  $k$  will deteriorate the clustering results.

Taking ORL as an example, we show the effects of  $\alpha$  and  $k$  on clustering performance in Figs. 4 and 5. We observe similar patterns on them. First, for a fixed  $k$ , the performance is enhanced when  $\alpha$  increases. However, the performance is degraded when  $\alpha$  has a large value. Second, it is easy to achieve good performance with a small  $k$ . Overall, a reasonable result can be achieved with a small range of  $k$  and a large range of  $\alpha$ .

#### 4.5 Comparison with Deep Methods

Motivated by the success of deep neural networks (DNNs), unsupervised deep learning approaches are now widely used to learn

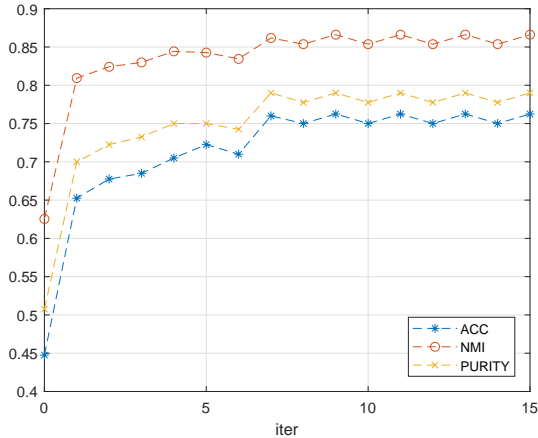


Figure 3: The variation of performance throughout the iteration on ORL dataset.

nonlinear mappings from the data domain to low-dimensional latent spaces, which are supposed to be naturally suitable for clustering. Though our work is based on similar assumptions, we use the simple graph filtering technique instead.

We compare with some state-of-the-art deep clustering techniques, including SSC with pre-trained convolutional auto-encoder features (AE+SSC), Deep Subspace Clustering Network with L1-norm (DSC-L1) [10], Deep Embedding Clustering (DEC) [38], and Deep K-means (DKM) [5], Deep Comprehensive Correlation Mining (DCCM) [37]. In particular, DSC-L1 implements subspace clustering with DNNs and is closely related to our work. For a fair comparison, we directly copy the reported results for AE-SSC and DSC-L1 from [10, 46]. For DEC, DKM, DCCM, we use the same encoder-decoder architecture in DEC [38] and DKM [5].

Table 5 shows the results given by various methods. We can observe the followings.

- 1) FTRR outperforms the strongest baseline DSC-L1 on ORL and Umist, and is inferior to DSC-L1 on COIL40, COIL20, and MNIST. Wilcoxon signed rank test gives a  $p$  value of 0.56, thus FTRR and DSC-L1 are not statistically different from each other. Considering the complexity of training DNNs, graph filtering based subspace clustering is more appealing in practice.
- 2) FLSR generally outperforms DEC and DKM. FLSR also outperforms the most recent DCCM method on ORL, Umist, and MNIST. This shows that our learned representation is easy to cluster.
- 3) FTRR consistently outperforms DEC, DKM, and DCCM by a very large margin. This clearly demonstrate the effectiveness of graph filtering technique.

In summary, compared to deep clustering techniques, graph filtering approach is not only simple but also effective. From this perspective, our work falls into a family of recent efforts questioning the systematic use of complex deep learning methods without clear comparison to less fancy but simpler baselines [2, 17]. Our approach can be a simpler alternative to deep clustering methods.

## 5 ABLATION STUDY

Though we have demonstrated that graph filtering can improve the separability of raw data in Fig.1, we further analyze this quantitatively. In particular, we also show that graph filtering has the effect of denoising, which also contributes to the performance improvement of downstream tasks. Taking COIL40 as an example, we add Gaussian noise with mean 1 and variance  $\sigma = 0.05$  to the raw features. Rather than using an iterative approach in our algorithm, we build the affinity graph using the probabilistic k-nearest method [25]. With this prior graph, it is easy to examine the effect of different orders of filter.

We first apply three metrics to systematically analyze the effect of filtering. Peak Signal to Noise Ratio (PSNR) is a standard measure for denoising, which relies strictly on numeric comparison. Structural Similarity Index (SSIM) [35] is a popular metric to evaluate the structural similarities between images. Higher PSNR and SSIM indicate that the reconstruction is of higher quality with respect to the original images. Besides, we want to directly see how well graph filtering can separate samples in different clusters. Fisher Score [6] is a traditional metric to measure the linear separability of two sets of features. Thus, we can use it to evaluate the separability of data space before and after filtering. Therefore, higher Fisher Score indicates the feature space is more “clustering-friendly”.

For two clusters of samples  $X^i$  and  $X^j$ , Fisher Score is calculated as the ratio of the variance between the classes (inter-class distance) to the variance within the classes (inner-class distance) under the best linear projection  $\mathbf{w}$  of the original feature:

$$J\left(X^{(i)}, X^{(j)}\right) = \max_{\mathbf{w} \in \mathbb{R}^m} \frac{\left(\mathbf{w}^\top \left(\boldsymbol{\mu}^{(i)} - \boldsymbol{\mu}^{(j)}\right)\right)^2}{\mathbf{w}^\top \left(\boldsymbol{\Sigma}^{(i)} + \boldsymbol{\Sigma}^{(j)}\right) \mathbf{w}} \quad (13)$$

where  $\boldsymbol{\mu}^{(i)}$  and  $\boldsymbol{\mu}^{(j)}$  represent the mean vector of  $X^i$  and  $X^j$  respectively,  $\boldsymbol{\Sigma}^{(i)}$  and  $\boldsymbol{\Sigma}^{(j)}$  represent the variance of  $X^i$  and  $X^j$  respectively. We can see that a larger  $J$  indicates higher separability. It is known that the maximum separation occurs when  $\mathbf{w} = c \left(\boldsymbol{\Sigma}^{(i)} + \boldsymbol{\Sigma}^{(j)}\right)^{-1} \left(\boldsymbol{\mu}^{(i)} - \boldsymbol{\mu}^{(j)}\right)$ , where  $c$  is a scalar. Plugging this into Eq.(13), we obtain

$$J\left(X^{(i)}, X^{(j)}\right) = \left(\boldsymbol{\mu}^{(i)} - \boldsymbol{\mu}^{(j)}\right)^\top \left(\boldsymbol{\Sigma}^{(i)} + \boldsymbol{\Sigma}^{(j)}\right)^{-1} \left(\boldsymbol{\mu}^{(i)} - \boldsymbol{\mu}^{(j)}\right).$$

Then we perform graph filtering on both noisy data and raw data from  $k = 1$  to  $k = 10$ . For each  $k$ , we compute the PSNR, SSIM, Fisher Score for each sample and report the average value in Table 4. We can observe that PSNR, SSIM, and Fisher Score share the same trend, i.e., they increase when  $k$  becomes larger at the beginning, then begin to drop when  $k$  becomes too big. As mention earlier, this indicates that too large  $k$  will incur over-smoothing. Specifically, PSNR jumps from 26.12 to 28.76 when we apply graph filter  $k = 1$  to the noisy images. For SSIM, it reaches its peak when  $k = 3$ . These verify that graph filtering has the effect of removing noise and recovering the structure of images. This echos the findings in Fig.2. Fisher Score reaches its peak when  $k = 5$ , which validates that graph filtering enhances separability of data representation.

We visualize two sample images in Fig.6. We can observe that all images become smoother when the  $k$  increases. From the second and fourth row, it can see that noise is reduced from left to right. As a matter of fact, a natural image can be decomposed into a low

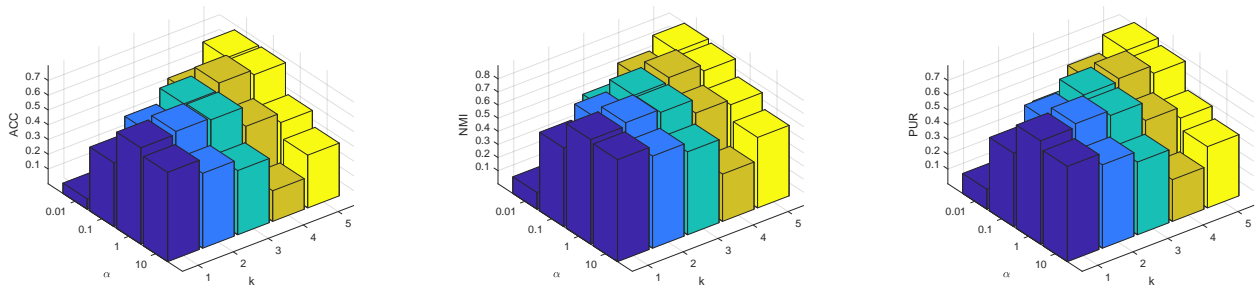


Figure 4: The influence of parameters  $\alpha$  and  $k$  for FLSR on ORL dataset.

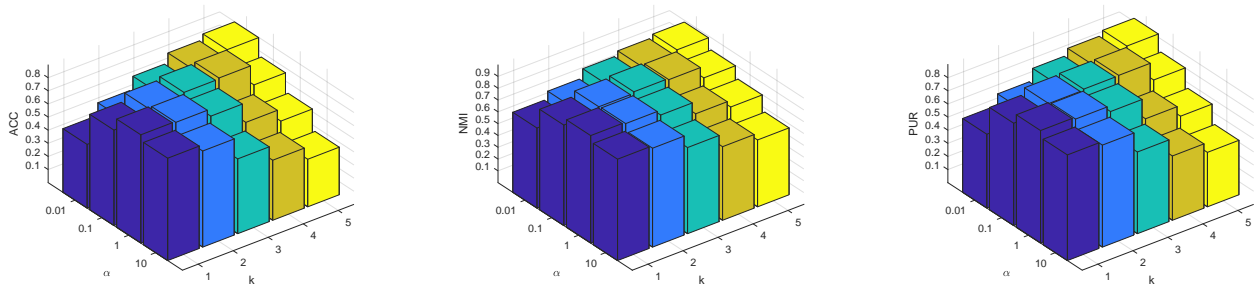


Figure 5: The influence of parameters  $\alpha$  and  $k$  for FTRR on ORL dataset.

Table 4: The detailed analysis of the influence of filter order  $k$  on PSNR, SSIM, and Fisher Score for noisy COIL40 data.

Metric	Corrupted	$k = 1$	$k = 2$	$k = 3$	$k = 4$	$k = 5$	$k = 6$	$k = 7$	$k = 8$	$k = 9$	$k = 10$
PSNR	26.12	28.76	28.30	27.76	27.34	27.02	26.75	26.52	26.32	26.15	25.99
SSIM	0.6995	0.8193	0.8435	0.8477	0.8477	0.8463	0.8444	0.8423	0.8400	0.8377	0.8354
Fisher Score	$8.8 \times 10^4$	$1.5 \times 10^6$	$1.1 \times 10^7$	$4.0 \times 10^7$	$9.0 \times 10^7$	$1.6 \times 10^8$	$1.6 \times 10^8$	$6.5 \times 10^7$	$4.0 \times 10^7$	$3.0 \times 10^7$	$2.2 \times 10^7$

Table 5: Clustering results on raw and filtered feature space of COIL40 dataset.

Data	Metric	Unfiltered	$k = 1$	$k = 2$	$k = 3$	$k = 4$	$k = 5$	$k = 6$	$k = 7$	$k = 8$	$k = 9$	$k = 10$
Raw	ACC	77.81	82.19	91.04	91.22	92.85	92.99	91.67	92.26	<b>93.40</b>	93.09	92.33
	NMI	88.20	90.19	95.41	95.15	96.41	96.35	96.42	96.48	<b>96.97</b>	96.75	96.44
	PUR	81.67	84.20	91.98	91.70	93.33	93.06	93.26	93.40	<b>94.51</b>	94.20	93.44
Corrupted	ACC	71.32	86.29	90.90	91.91	91.81	92.01	92.01	92.08	93.06	<b>93.13</b>	92.05
	NMI	84.81	92.78	95.78	95.90	95.94	96.24	96.15	96.20	96.69	<b>96.80</b>	96.01
	PUR	77.57	87.81	92.33	92.40	92.88	93.13	93.13	93.00	94.27	<b>94.27</b>	92.92

spatial frequency component and a high spatial frequency part. The former contains the smoothly changing structure, e.g., background, and the latter one describes the rapidly changing fine details, e.g., outliers. This explains why our low-pass filter can help remove the noise. Too large  $k$  will remove some specific properties of classes, which results in non-discriminative representations. This in turn

makes it hard to separate those images, resulting in a decline in performance.

Table 5 further reports the clustering results under different  $k$ . Similarly, we can see that the performance increases until  $k$  reaches 8 and 9 for raw and corrupted data, respectively. Though there is 6.5 gap on clustering accuracy between raw and corrupted data, we achieve similar performance after we introduce the graph filtering.

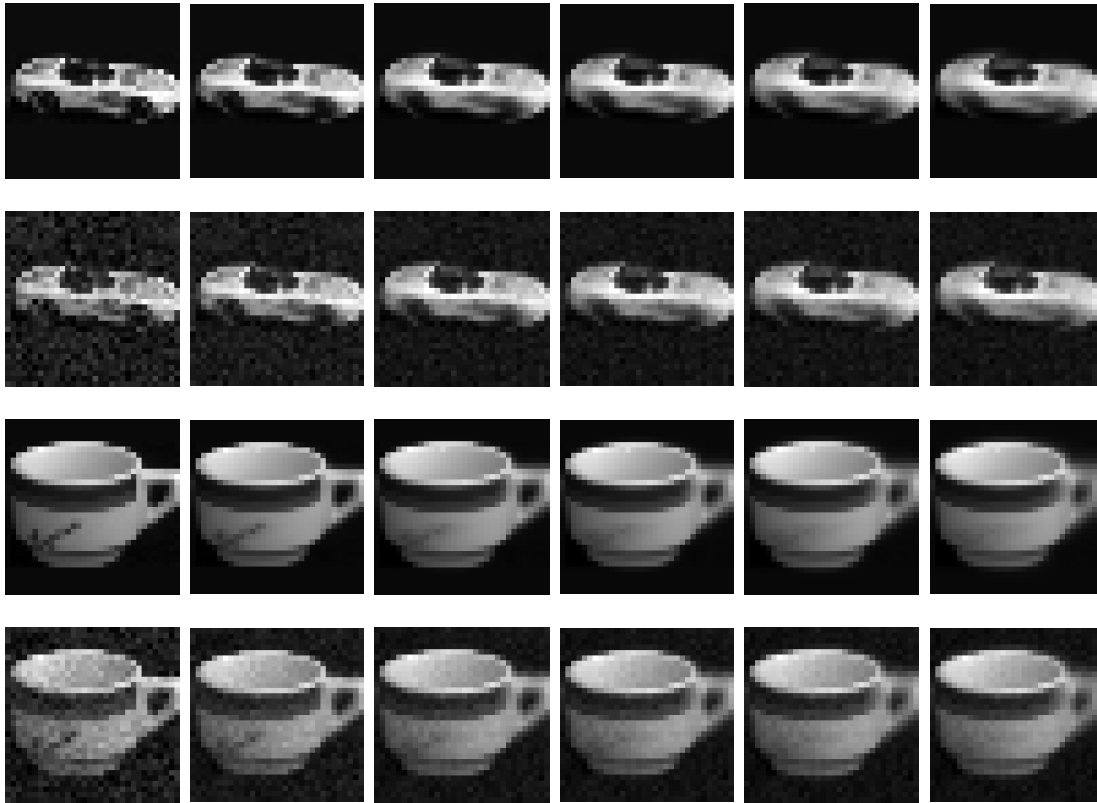


**Figure 6: Samples of images before and after graph filtering. Rows 1&3 are two raw images while rows 2&4 are their corresponding noisy images. From left to right, each column corresponds to filter order  $k = 0$  (unfiltered), 1, 3, 5, 7 and 10.**

Furthermore, the reported performance on COIL40 is much better than that in Tables 2 and 5. This is due to the fact that we use a different graph construction method [25], which consequently produces high quality graph filtering. It has been proved that an ideal graph should consist of  $g$ -connected components [14]. [25] harnesses this nice property and proposes a rank constrained graph construction method. From this perspective, our performance in Table 2 could be further improved if a prior graph with high-quality is available in advance. Of course, we must combine the best of both worlds. Without graph filtering, [25] generates clustering performance 0.8392, 0.9250, 0.8722, in terms of accuracy, NMI, purity, respectively. This is inferior to our performance.

## 6 CONCLUSION

In this paper, we make the first attempt to introduce graph filtering to subspace clustering. Our goal is to perform subspace clustering in a “clustering-friendly” representation, i.e., the data representation displays cluster structure, which in turn facilitates the downstream clustering. This is realized by graph filtering technique. Since the graph is unavailable beforehand, we adopt an iterative strategy. Taking LSR and TRR benchmark as examples, we show the considerable improvements brought by the smooth representation on

seven datasets. Moreover, we demonstrate that graph filtering approach reaches comparable performance as deep learning methods. An ablation study demonstrates that graph filtering can remove noise, preserve structure in the image, and increase the separability of classes. In the future, we can utilize the graph filtering in a wider scope, e.g., classification and semi-supervised learning.

## ACKNOWLEDGMENTS

This paper was in part supported by Grants from the Natural Science Foundation of China (No. 61806045), the National Key R&D Program of China (No. 2018YFC0807500), the Fundamental Research Fund for the Central Universities under Project ZYGX2019Z015, the Sichuan Science and Technology Program (Nos. 2020YFS0057, 2019YFG0202), the Ministry of Science and Technology of Sichuan Province Program (Nos. 2018GZDZX0048, 20ZDYF0343, 2018GZDZX0014, 2018GZDZX0034).

## REFERENCES

- [1] Fan RK Chung and Fan Chung Graham. 1997. *Spectral graph theory*. Number 92. American Mathematical Soc.
- [2] Maurizio Ferrari Dacrema, Paolo Cremonesi, and Dietmar Jannach. 2019. Are we really making much progress? A worrying analysis of recent neural recommendation approaches. In *Proceedings of the 13th ACM Conference on Recommender Systems*. 101–109.



- [3] Ehsan Elhamifar and René Vidal. 2009. Sparse subspace clustering. In *2009 IEEE Conference on Computer Vision and Pattern Recognition*. IEEE, 2790–2797.
- [4] Levent Ertöz, Michael Steinbach, and Vipin Kumar. 2003. Finding clusters of different sizes, shapes, and densities in noisy, high dimensional data. In *Proceedings of the 2003 SIAM international conference on data mining*. SIAM, 47–58.
- [5] Maziar Moradi Fard, Thibaut Thonet, and Eric Gaussier. 2018. Deep  $k$ -Means: Jointly clustering with  $k$ -Means and learning representations. *arXiv preprint arXiv:1806.10069* (2018).
- [6] Ronald A Fisher. 1936. The use of multiple measurements in taxonomic problems. *Annals of eugenics* 7, 2 (1936), 179–188.
- [7] Han Hu, Zhouchen Lin, Jianjiang Feng, and Jie Zhou. 2014. Smooth representation clustering. In *Proceedings of the IEEE Conference on Computer Vision and Pattern Recognition*. 3834–3841.
- [8] Rongyao Hu, Xingyi Liu, Cheng debo, Wei He, and Luo Yan. 2017. Robust Low-rank Self-representation Feature Selection Algorithm. *Computer Engineering* 43, 9 (2017), 43–50.
- [9] Pan Ji, Mathieu Salzmann, and Hongdong Li. 2015. Shape interaction matrix revisited and robustified: Efficient subspace clustering with corrupted and incomplete data. In *Proceedings of the IEEE International Conference on computer vision*. 4687–4695.
- [10] Pan Ji, Tong Zhang, Hongdong Li, Mathieu Salzmann, and Ian Reid. 2017. Deep subspace clustering networks. In *Advances in Neural Information Processing Systems*. 24–33.
- [11] Zhao Kang, Xiao Lu, Jian Liang, Kun Bai, and Zenglin Xu. 2020. Relation-Guided Representation Learning. *Neural Networks* (2020). <https://doi.org/10.1016/j.neunet.2020.07.014>
- [12] Zhao Kang, Xiao Lu, Yiwei Lu, chong Peng, Wenyu Chen, and Zenglin Xu. 2020. Structure Learning with Similarity Preserving. *Neural Networks* 129 (2020), 138–148.
- [13] Zhao Kang, Haiqi Pan, Steven C.H. Hoi, and Zenglin Xu. 2020. Robust Graph Learning From Noisy Data. *IEEE Transactions on Cybernetics* 50, 5 (2020), 1833–1843.
- [14] Zhao Kang, Chong Peng, and Qiang Cheng. 2017. Twin Learning for Similarity and Clustering: A Unified Kernel Approach. In *AAAI*. 2080–2086.
- [15] Zhao Kang, Wangtao Zhou, Zhitong Zhao, Junming Shao, Meng Han, and Zenglin Xu. 2020. Large-scale Multi-view Subspace Clustering in Linear Time. In *Thirty-Fourth AAAI Conference on Artificial Intelligence*. 4412–4419.
- [16] Chun-Guang Li, Chong You, and René Vidal. 2017. Structured sparse subspace clustering: A joint affinity learning and subspace clustering framework. *IEEE Transactions on Image Processing* 26, 6 (2017), 2988–3001.
- [17] Jimmy Lin. 2019. The neural hype and comparisons against weak baselines. In *ACM SIGIR Forum*, Vol. 52. ACM New York, NY, USA, 40–51.
- [18] Guangcan Liu, Zhouchen Lin, and Yong Yu. 2010. Robust subspace segmentation by low-rank representation. In *ICML*, Vol. 1. 8.
- [19] Guangcan Liu and Shuicheng Yan. 2011. Latent low-rank representation for subspace segmentation and feature extraction. In *2011 International Conference on Computer Vision*. IEEE, 1615–1622.
- [20] Guangcan Liu, Zhao Zhang, Qingshan Liu, and Hongkai Xiong. 2019. Robust subspace clustering with compressed data. *IEEE Transactions on Image Processing* 28, 10 (2019), 5161–5170.
- [21] Xinwang Liu, Miaomiao Li, Chang Tang, Jingyuan Xia, Jian Xiong, Li Liu, Marius Kloft, and En Zhu. 2020. Efficient and effective regularized incomplete multi-view clustering. *IEEE Transactions on Pattern Analysis and Machine Intelligence* (2020).
- [22] Stuart Lloyd. 1982. Least squares quantization in PCM. *IEEE transactions on information theory* 28, 2 (1982), 129–137.
- [23] Can-Yi Lu, Hai Min, Zhong-Qiu Zhao, Lin Zhu, De-Shuang Huang, and Shuicheng Yan. 2012. Robust and efficient subspace segmentation via least squares regression. In *European conference on computer vision*. Springer, 347–360.
- [24] Andrew Y Ng, Michael I Jordan, and Yair Weiss. 2002. On spectral clustering: Analysis and an algorithm. In *Advances in neural information processing systems*. 849–856.
- [25] Feiping Nie, Xiaoqian Wang, Michael I. Jordan, and Heng Huang. 2016. The Constrained Laplacian Rank Algorithm for Graph-Based Clustering. In *Proceedings of the Thirtieth AAAI Conference on Artificial Intelligence* (Phoenix, Arizona) (AAAI’16). AAAI Press, 1969–1976.
- [26] Vishal M Patel, Hien Van Nguyen, and René Vidal. 2015. Latent space sparse and low-rank subspace clustering. *IEEE Journal of Selected Topics in Signal Processing* 9, 4 (2015), 691–701.
- [27] Chong Peng, Zhao Kang, Shuting Cai, and Qiang Cheng. 2018. Integrate and conquer: Double-sided two-dimensional  $k$ -means via integrating of projection and manifold construction. *ACM Transactions on Intelligent Systems and Technology (TIST)* 9, 5 (2018), 1–25.
- [28] Chong Peng, Zhao Kang, Yunhong Hu, Jie Cheng, and Qiang Cheng. 2017. Non-negative matrix factorization with integrated graph and feature learning. *ACM Transactions on Intelligent Systems and Technology (TIST)* 8, 3 (2017), 1–29.
- [29] Xi Peng, Zhang Yi, and Huajin Tang. 2015. Robust subspace clustering via thresholding ridge regression. In *Twenty-Ninth AAAI Conference on Artificial Intelligence*.
- [30] David I Shuman, Sunil K Narang, Pascal Frossard, Antonio Ortega, and Pierre Vandergheynst. 2013. The emerging field of signal processing on graphs: Extending high-dimensional data analysis to networks and other irregular domains. *IEEE signal processing magazine* 30, 3 (2013), 83–98.
- [31] René Vidal. 2011. Subspace clustering. *IEEE Signal Processing Magazine* 28, 2 (2011), 52–68.
- [32] René Vidal and Paolo Favaro. 2014. Low rank subspace clustering (LRSC). *Pattern Recognition Letters* 43 (2014), 47–61.
- [33] Xing Wang and Zhao Kang. 2021. Smooth representation semi-supervised classification. *Computer Science* 48, 3 (2021).
- [34] Xiaoqian Wang, Yun Liu, Feiping Nie, and Heng Huang. 2015. Discriminative unsupervised dimensionality reduction. In *Twenty-Fourth International Joint Conference on Artificial Intelligence*.
- [35] Z. Wang, A. C. Bovik, H. R. Sheikh, and E. P. Simoncelli. 2004. Image Quality Assessment: From Error Visibility to Structural Similarity. *IEEE Transactions on Image Processing* 13, 4 (April 2004), 600–612. <https://doi.org/10.1109/TIP.2003.819861>
- [36] Jie Wen, Zheng Zhang, Zhao Zhang, Lunke Fei, and Meng Wang. 2020. Generalized Incomplete Multiview Clustering With Flexible Locality Structure Diffusion. *IEEE Transactions on Cybernetics* (2020).
- [37] Jianlong Wu, Keyu Long, Fei Wang, Chen Qian, Cheng Li, Zhouchen Lin, and Hongbin Zha. 2019. Deep Comprehensive Correlation Mining for Image Clustering. In *The IEEE International Conference on Computer Vision (ICCV)*.
- [38] Junyuan Xie, Ross Girshick, and Ali Farhadi. 2016. Unsupervised deep embedding for clustering analysis. In *International conference on machine learning*. 478–487.
- [39] Jun Xu, Mengyang Yu, Ling Shao, Wangmeng Zuo, Deyu Meng, Lei Zhang, and David Zhang. 2019. Scaled Simplex Representation for Subspace Clustering. *IEEE Transactions on Cybernetics* (2019).
- [40] Chong You, Chi Li, Daniel P Robinson, and René Vidal. 2018. Scalable exemplar-based subspace clustering on class-imbalanced data. In *Proceedings of the European Conference on Computer Vision (ECCV)*. 67–83.
- [41] Chong You, Chun-Guang Li, Daniel P Robinson, and René Vidal. 2016. Oracle based active set algorithm for scalable elastic net subspace clustering. In *Proceedings of the IEEE conference on computer vision and pattern recognition*. 3928–3937.
- [42] Chong You, Daniel Robinson, and René Vidal. 2016. Scalable sparse subspace clustering by orthogonal matching pursuit. In *Proceedings of the IEEE conference on computer vision and pattern recognition*. 3918–3927.
- [43] Changqing Zhang, Huazhu Fu, Qinghua Hu, Xiaochun Cao, Yuan Xie, Dacheng Tao, and Dong Xu. 2020. Generalized latent multi-view subspace clustering. *IEEE transactions on pattern analysis and machine intelligence* 42, 1 (2020), 86–99.
- [44] Xiaotong Zhang, Han Liu, Qimai Li, and Xiao-Ming Wu. 2019. Attributed Graph Clustering via Adaptive Graph Convolution. In *the 28th International Joint Conference on Artificial Intelligence*.
- [45] Zhao Zhang, Yan Zhang, Sheng Li, Guangcan Liu, Dan Zeng, Shuicheng Yan, and Meng Wang. 2019. Flexible auto-weighted local-coordinate concept factorization: A robust framework for unsupervised clustering. *IEEE Transactions on Knowledge and Data Engineering* (2019).
- [46] Pan Zhou, Yunqing Hou, and Jiashi Feng. 2018. Deep adversarial subspace clustering. In *Proceedings of the IEEE Conference on Computer Vision and Pattern Recognition*. 1596–1604.